Supporting Information

The role of structural and energetic factors in regulating repair of a bulky DNA lesion with different opposite partner bases

Hong Mu [||, ‡], Konstantin Kropachev [||, §], Ying Chen [§], Hong Zhang [‡], Yuqin Cai[‡], Nicholas E. Geacintov *[, §] and Suse Broyde*[, ‡]

[‡]*Department of Biology and* [§]*Department of Chemistry, New York University, New York, NY 10003, USA.*

TABLE OF CONTENTS

SUPPORTING FIGURES

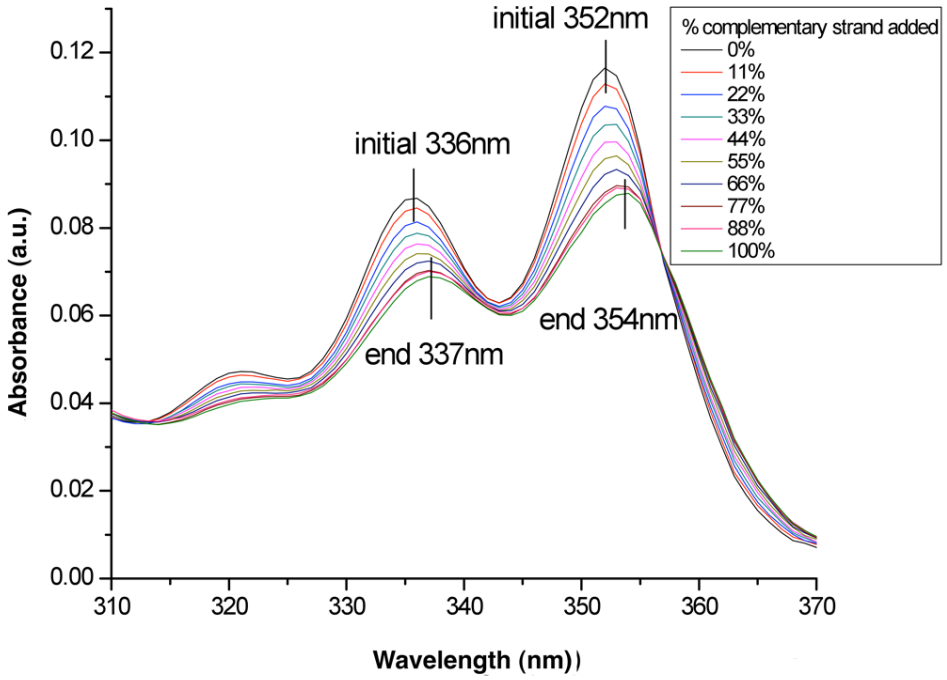

Figure S1. UV absorption titration curves of the *cis*-B[*a*]P-dG:dT duplex exhibit red-shifted and decreased absorption maxima, indicating an intercalated conformation of the lesion. The initial absorption spectrum represents the absorbance of the single stranded lesion-containing oligonucleotide with vibronic absorption maxima at 336 and 352 nm. The lowest trace ('end' of the titration of a solution of the modified strand with 1:1 modified:unmodified strand ratio, '100%') represents the absorption spectrum of the full duplex with red-shifted absorption maxima to 337 and 354 nm, respectively (1). The titration method is fully described in (2).

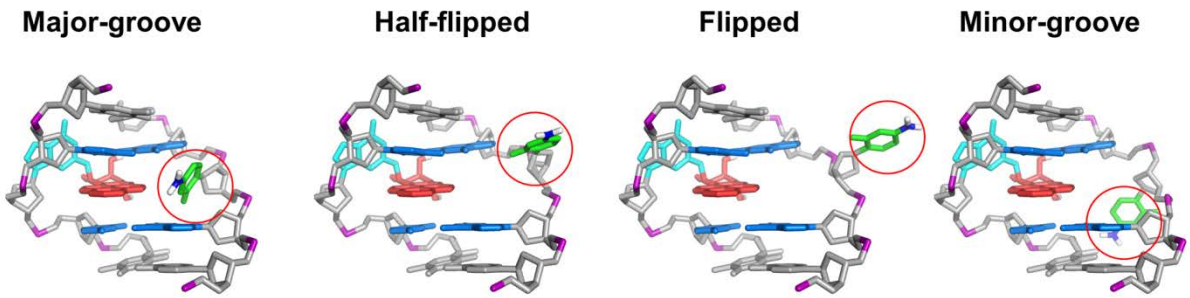

Figure S2. The four initial positions of the partner bases modeled for our conformational searches of partner conformations in the damaged duplexes. Shown are the central 5-mers of the initial structures for the *cis*-B[*a*]P-dG:dC duplex. The partner bases are highlighted in red circles. The structures are viewed from the major groove side and represented in sticks: hydrogen and phosphate oxygen atoms are deleted for clarity, except for the hydrogen atoms of the hydroxyl groups for the benzylic ring and those of the amino group of the partner C. The lesion-containing strands and the complementary strands are in light gray. The B[*a*]P rings are red. The modified guanine is cyan and partner C is green, and the neighboring bases are marine blue. The phosphates are purple, the hydrogen atoms are white and the nitrogen atom of the amino group of the partner C is blue.

A Normal partner C duplex

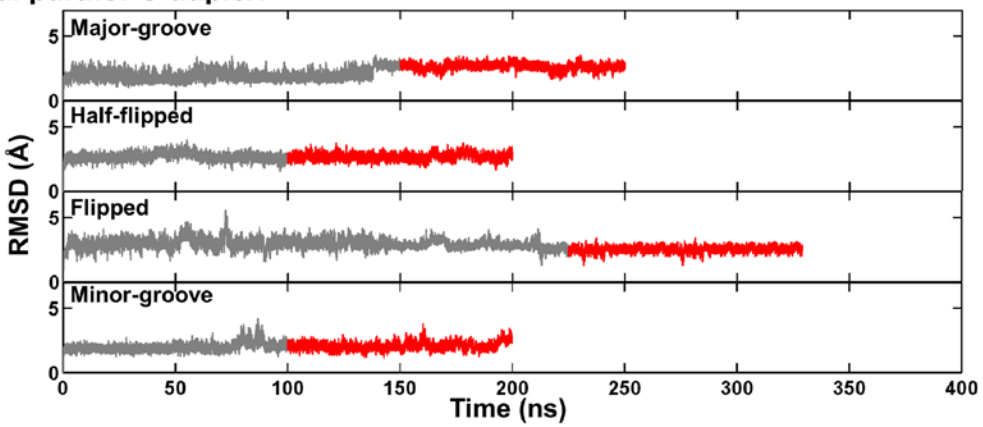

B Mismatched partner T duplex

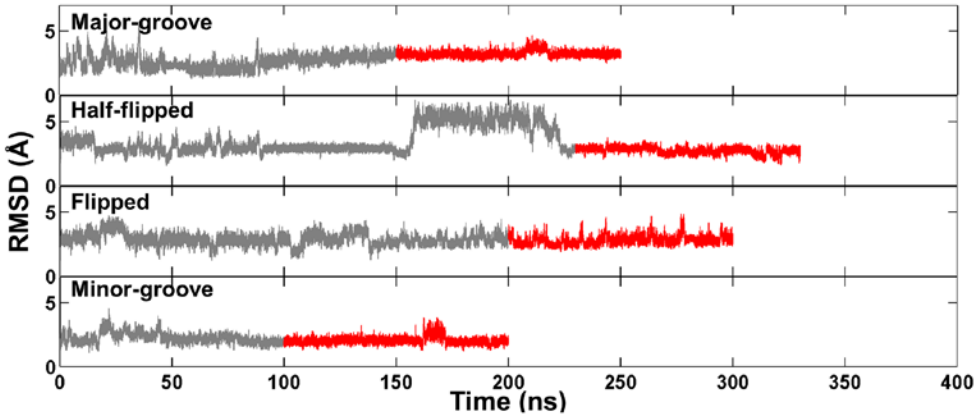

C Mismatched partner A duplex

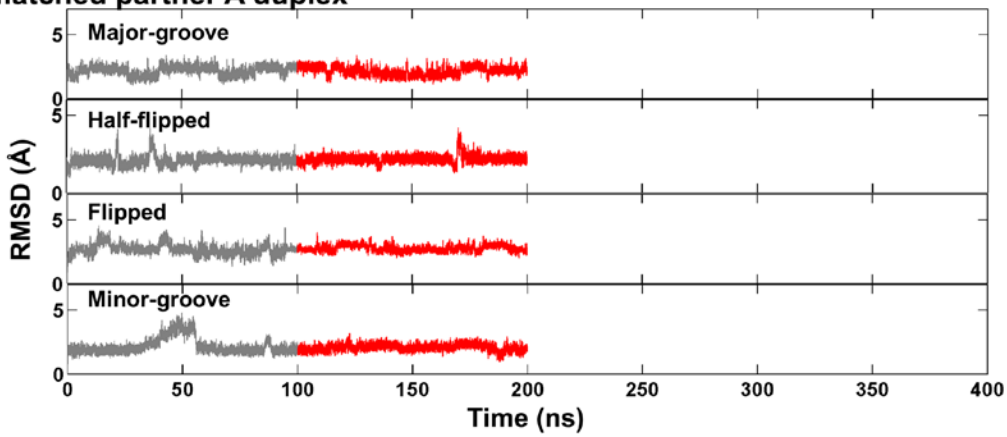

D Mismatched partner G duplex

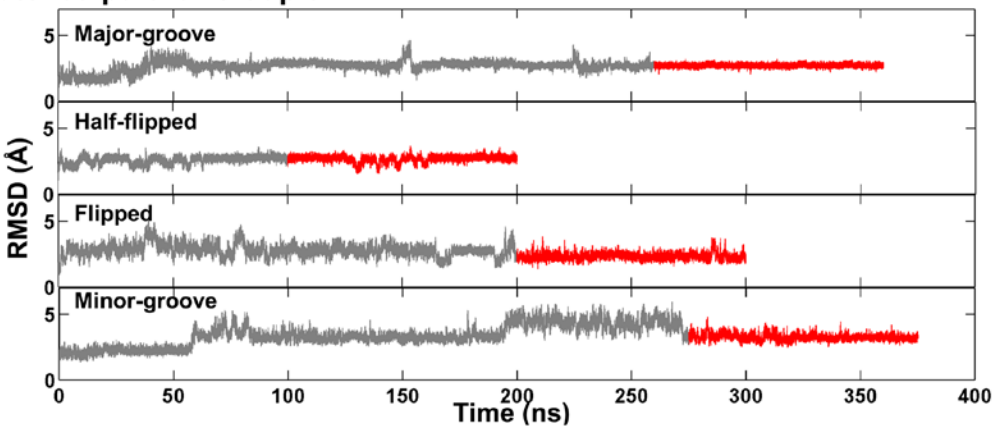

Figure S3. The time dependent central 5-mer RMSD against the first frame for all simulated duplexes. The starting positions of the partner base, Major-groove, Half-flipped, Flipped and Minor-groove positions (Figure S2), are labeled at the top left corner of the respective plots. The RMSD of the 100 ns stable structural ensembles for each simulated duplex are in red. (A) The *cis*-B[*a*]P-dG:dC duplex. (B) The *cis*-B[*a*]P-dG:dT duplex. (C) The *cis*-B[*a*]P-dG:dA duplex. (D) The *cis*-B[*a*]P-dG:dG duplex.

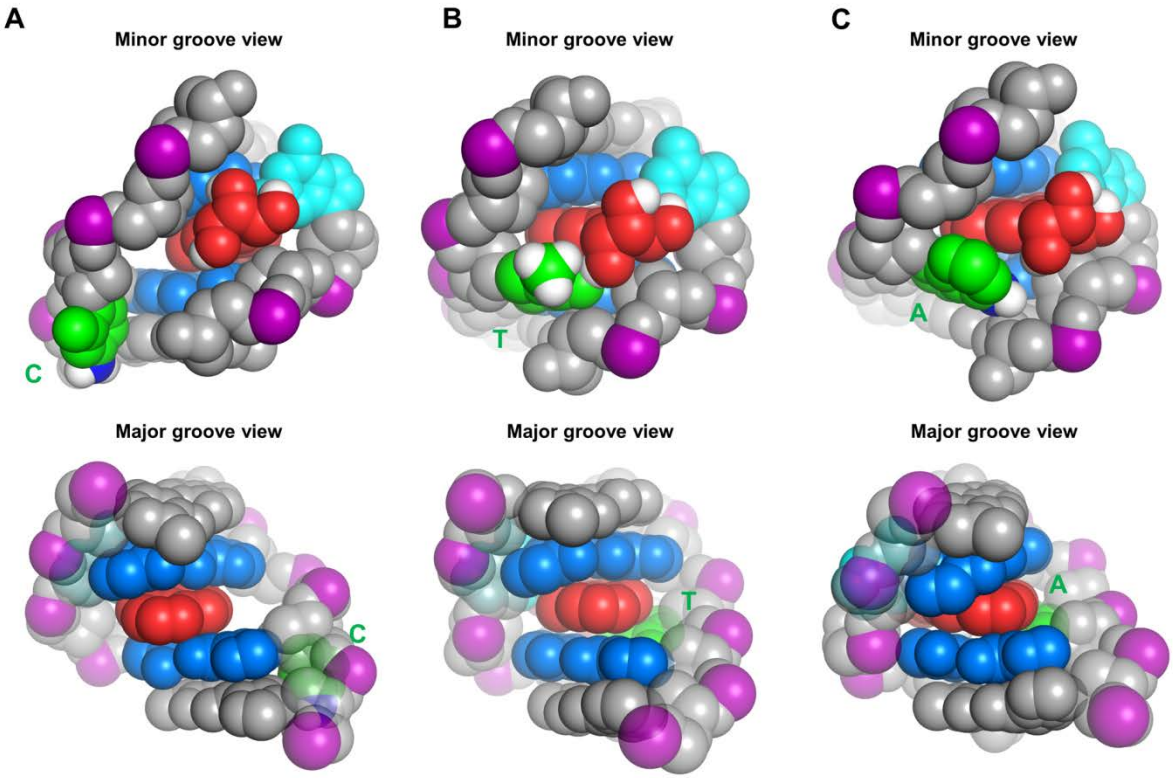

Figure S4. The best representative structures of the less probable minor groove conformations for the *cis*-B[*a*]P-dG:dC, dT and dA duplexes. The central 5-mers are represented in CPK, colored as in Figure S2, and viewed from both minor and major groove sides. When viewed from the major groove side, the backbone atoms are rendered in transparent CPK to reveal the displaced bases in the minor groove. (A) The *cis*-B[*a*]P-dG:dC duplex. (B) The *cis*-B[*a*]P-dG:dT duplex. (C) The *cis*-B[*a*]P-dG:dA duplex.

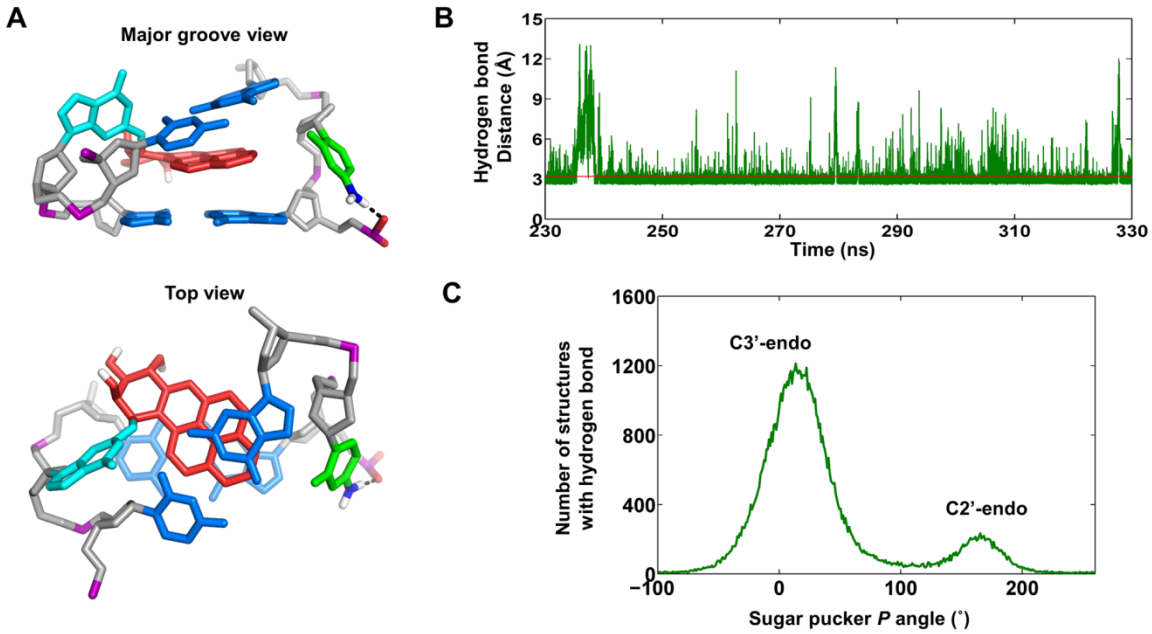

Figure S5. Partner dC is very dynamic and extruded: a dynamic hydrogen bond controls the sugar pucker and the extent of extrusion. (A) The most representative structure for the *cis*-B[*a*]P-dG:dC duplex with partner dC in C3'-endo sugar pucker conformation. The central trimer is rendered as in Figure S2 and viewed from the major groove (Major groove view) and along the helix axis (Top view). (B) The dynamics of the hydrogen bond distance between the amino group nitrogen atom of the partner dC and the pendant phosphate oxygen atom. (C) The distribution of the sugar pucker pseudo-rotation phase angle (*P* angle) (3) of the partner dC for the structures with hydrogen bond between dC and the pendant phosphate oxygen atom, showing the strong correlation between hydrogen bond formation and C3'-endo sugar pucker of the dC. When the hydrogen bond is present, the sugar pucker of the dC-deoxyribose is predominantly in the C3'-endo domain, where the distance between the hydrogen bonding partners is short enough for the hydrogen bond to form with mean value of 2.9Å for heavy atom to heavy atom distance; however, when the pucker is C2'-endo the distance is usually too long for hydrogen bonding with mean value of 4.2Å.

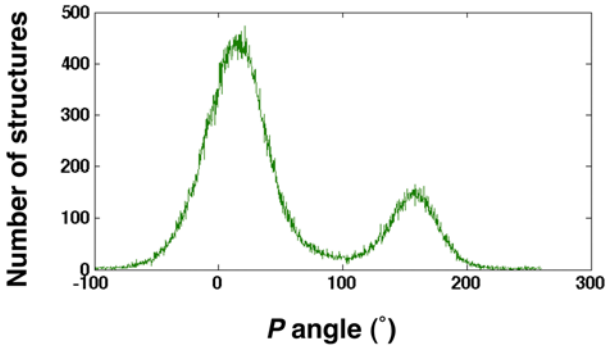

Figure S6. The population distribution of the sugar pucker pseudorotation phase angle (*P* angle) (3) of partner dC reveals a minor population (15%) with C2'-endo conformation. The population was determined by using the kmeans clustering method of MATLAB (4) with cluster number at 2 and replicates at 10. This minor population is more extruded as seen in Figure 1 of the main text.

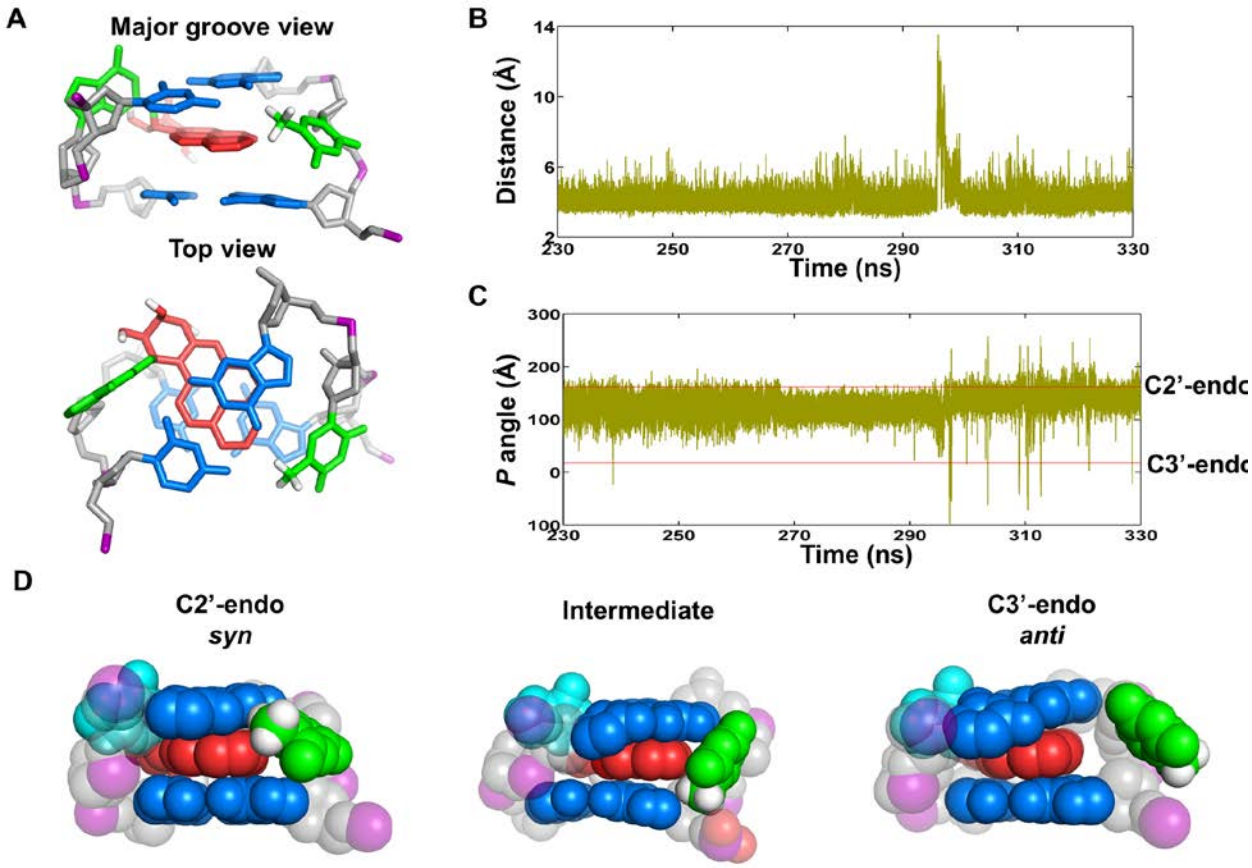

Figure S7. Hydrophobic thymine methyl promotes interaction of dT with major groove surface. (A) The most representative structure for the *cis*-B[*a*]P-dG:dT duplex. The central trimer is rendered as in Figure S2 and viewed from the major groove (Major groove view) and along the helix axis (Top view). (B) The dynamics of the distance between the methyl group carbon atom of the partner dT and the most distal carbon atom of the B[*a*]P. The fraction of the population with distance greater than 6Å is 2%. (C) The dynamics of the sugar pucker pseudo-rotation phase angle (*P* angle) of the partner dT. (D) The representative structures (in CPK) showing the C2'-endo and C3'-endo sugar pucker transitions of the partner dT for the *cis*-B[*a*]P-dG:dT duplex. The phosphate oxygen atoms of dG16 are also shown in red spheres to highlight steric crowding between the partner T methyl group and the backbone in the intermediate stage between *syn* and *anti* conformations, that promotes the rare and temporary extrusion of the thymine.

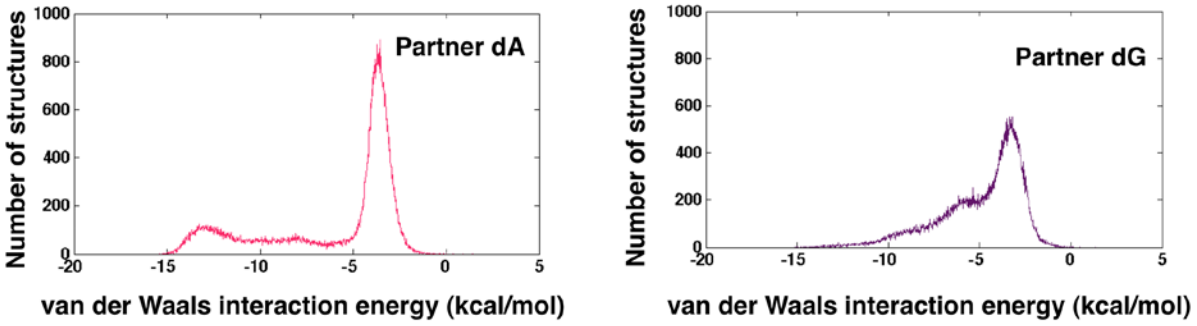

Figure S8. The population distributions of the van der Waals interaction energies of partner bases A and G with adjacent base pairs reveals minor populations that are inserted (for A, population 23%) or partly-inserted (for G, population 31%). The van der Waals interaction energies were calculated as detailed in the Materials and Methods section. The distributions of the van der Waals interaction energies were obtained using the hist function of MATLAB (4) with number of bins set at 1000. The structural ensembles were clustered into two states since the distributions exhibit two significant populations for both partner A and partner G. The clustering was carried out using the kmeans function of MATLAB (4) with cluster number at 2 and repeat number at 10.

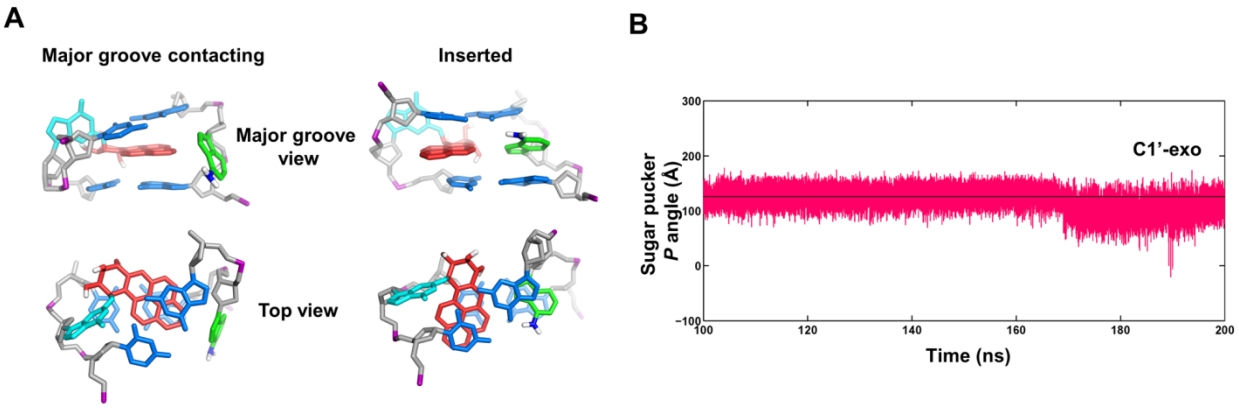

Figure S9. Partner dA adopts predominant major groove contacting conformation with a minor helix-inserted population. (A) The most representative structures for the *cis*-B[*a*]P-dG:dA duplex with partner dA in major groove contacting and inserted states. The central trimers are rendered as in Figure S2 and viewed from the major groove (Major groove view) and along the helix axis (Top view). (B) The dynamics of the sugar pucker pseudo-rotation phase angle (*P* angle) of the partner dA.

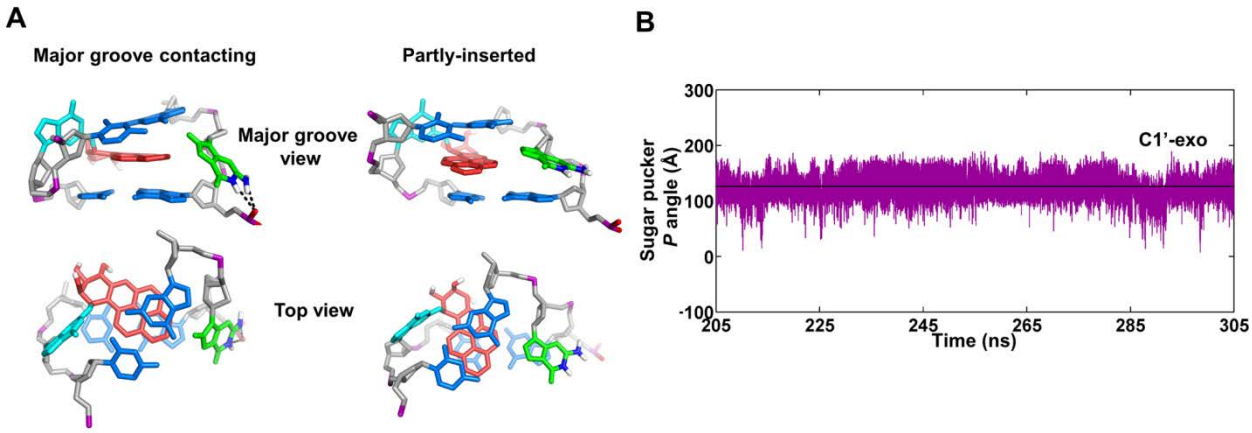

Figure S10. Partner dG adopts predominant major groove contacting conformation with a minor partly-inserted population. (A) The most representative structures for the *cis*-B[*a*]P-dG:dG duplex with partner dG in major groove contacting and partly-inserted states. The central trimers are rendered as in Figure S2 and viewed from the major groove (Major groove view) and along the helix axis (Top view). (B) The dynamics of the sugar pucker pseudo-rotation phase angle (*P* angle) of the partner dG.

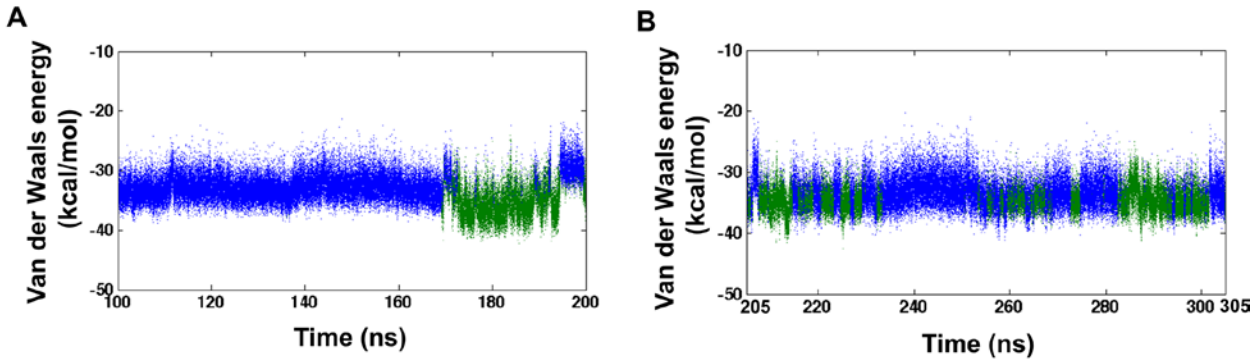

Figure S11. Time dependent values of the total interaction energy involving the intercalation pocket for the (A) *cis*-B[*a*]P-dG:dA and (B) *cis*-B[*a*]P-dG:dG duplexes reveal similar interaction energies for the major groove contacting and inserted/partly-inserted states of the partner base. The ensembles were clustered into the two states as described in Figure S8. The blue cluster represents the major groove contacting state, and the green one represents the inserted/partly-inserted one.

SUPPORTING TABLES

Table S1. Backbone torsion angles (degrees) that characterize the conformations of the sugar-phosphate backbone for the initial structures.

Backbone torsions [a]	**Major groove**	**Half-flipped**	**Flipped**	**Minor groove**
ζ (dG16)	-128	-128	-128	-174
α (dX17)	-67	-117	105	108
β (dX17)	-176	-154	151	122
γ (dX17)	53	133	9	-114
δ (dX17)	157	166	157	157
ε (dX17)	-161	174	83	154
ζ (dX17)	-146	175	-159	-39

a. Backbone torsion angles α, β, γ, δ, ε and ζ define sequentially the rotations around the covalent bonds along the sugar-phosphate backbone P→O5'→C5'→C4'→C3'→O3'→$P_{(n+1)}$, with α for the P→O5' rotation.

Table S2. Free energies of the partner conformations in the *cis*-B[*a*]P-dG-modified duplexes (central 5-mers) that evolved from each initial structure of the damaged duplexes. The energy rankings of the final structures and the convergence of different initial structures to similar final structures are given [a].

Duplex	Initial structure	Evolved structure	Free energy (kcal/mol)
***cis*-B[*a*]P-dG:dC**	Major groove	Major groove	-1462.15 (± 0.50)
	Half-flipped		-1458.48 (± 0.50)
	Flipped		-1461.48 (± 0.60)
	Minor groove	Minor groove	-1452.36 (± 0.51)
***cis*-B[*a*]P-dG:dT**	Major groove	Ruptured	-1307.64 (± 0.52)
	Half-flipped	Major groove	-1334.83 (± 0.49)
	Flipped		-1331.20 (± 0.56)
	Minor groove	Minor groove	-1332.90 (± 0.50)
***cis*-B[*a*]P-dG:dA**	Major groove	Major groove / inserted	-1376.27 (± 0.54)
	Half-flipped		-1377.20 (± 0.51)
	Flipped	Minor groove	-1372.67 (± 0.50)
	Minor groove		-1371.67 (± 0.50)
***cis*-B[*a*]P-dG:dG**	Major groove	Major groove / partly inserted	-1430.86 (± 0.51)
	Half-flipped		-1430.75 (± 0.48)
	Flipped		-1431.53 (± 0.49)
	Minor groove		-1429.62 (± 0.49)

a. Lowest energy structures are in red. Note that for the *cis*-B[*a*]P-dG:dC duplex three initial structures converged to the major groove conformation, which is lower energy than the minor groove structure; for the *cis*-B[*a*]P-dG:dT duplex two initial structures converged to the major groove conformation, which is lowest energy, one produced a minor groove conformation of higher energy and one led to a partly denatured duplex of very high energy; for the *cis*-B[*a*]P-dG:dA duplex two initial structures converged to the major groove contacting / inserted conformation (dominant population major groove contacting, minor population inserted), which is lowest in energy, and two initial structures converged to a minor groove conformation of higher energy; for the *cis*-B[*a*]P-dG:dG duplex all four initial structures converged to the major groove contacting / partly inserted conformation (dominant population major groove contacting, minor population partly inserted).

Table S3. Hydrogen bond occupancies involving the partner base and nearby DNA residues of the preferred conformations for the *cis*-B[*a*]P-dG-modified duplexes.

Duplex	Hydrogen bond	Occupancy (%)
***cis*-B[*a*]P-dG:dC**	N4 (dC17) – H4 (dC17)…O1P(dG16)	85
***cis*-B[*a*]P-dG:dG**	N1 (dG17) – H1 (dG17)…O1P(dG16)	51
	N2 (dG17) – H2 (dG17)…O1P(dG16)	69

SUPPORTING MATERIALS AND METHODS

Molecular modeling

Since the UV absorption spectra showed that the B[*a*]P rings in all mismatched duplexes adopt an intercalated conformation (1), the NMR structure of *cis*-B[*a*]P-dG in a normally paired DNA duplex (5) (Figure 1B in the main text), which exhibits a base-displaced intercalated conformation, was used as the initial basis of molecular modeling. The Watson-Crick partner C of the *cis*-B[*a*]P-dG in the normal DNA duplex was replaced with T, A or G to model the mismatched duplexes (Figure 1C in the main text). Since the conformations of the mismatched partner bases were not known, four initial positions for each of these partner bases were modeled (Figure S2): (1) Major-groove, where the partner base is slightly displaced towards the major groove as in the NMR solution structure of the *cis*-B[*a*]P-dG matched with C; (2) Half-flipped, where the partner base is flipped ~90˚ into the major groove; (3) Flipped, where the partner base is totally flipped out, pointing away from the backbone; and (4) Minor-groove, where the partner base is flipped all the way around the backbone into the minor groove. These models were created by rotating primarily backbone torsion angle ζ of the partner nucleotide dX17: C3' (dX17) – O3' (dX17) – P (dG18) – O5' (dG18), and subsequently adjusting other nearby torsions (Table S1) to provide structures with minimum collisions. These initial positions were selected to roughly divide the 360˚ around the DNA backbone into quartiles while also avoiding collisions. The normal Watson-Crick partner base C was also placed at these four positions and studied identically to benchmark our methods.

Molecular dynamics (MD) simulations

MD simulations with the partner base at each of the four positions, and for each *cis*-B[*a*]P-dG-modified duplex, were used to produce ensembles of structures that evolve to stable conformations. Thus, a total of 16 simulations were performed. MD simulations were carried out using the AMBER9 simulation package (6) with the Cornell *et al.* force field (7), the PARM99 parameter set (8) modified by parmbsc0 (9) and GAFF (10). Partial charges and added force field parameters for the *cis*-B[*a*]P-dG adduct were obtained from Mocquet *et al.* (11).

Each duplex was neutralized with Na^+ counterions and solvated with explicit water using the LEAP module of the AMBER 9 suite of programs (6). A rectangular periodic box of TIP3P water with 10.0 Å buffer was created around the DNA duplexes. The Particle-Mesh Ewald method with 9.0 Å cutoff for the non-bounded interactions was used in the energy minimizations and MD simulations.

Minimizations were carried out in two stages. First, 5000 steps of steepest descent minimization followed by 5000 cycles of conjugate gradient minimization were conducted for the water molecules and counterions with 500 $kcal \cdot mol^{-1} \cdot Å^{-2}$ restraint on the DNA. Then, 10000 steps of steepest descent minimization followed by 15000 cycles of conjugate gradient minimization were carried out on the whole system without restraints.

A 2.0 fs time step and the SHAKE algorithm were applied in the MD simulations. Each system was heated from 0 K to 300 K over 20 ps with the DNA fixed with a weak restraint of 10 $kcal \cdot mol^{-1} \cdot Å^{-2}$ at constant volume, using the Berendsen coupling algorithm (12) with a 1.0 ps coupling parameter. Each system was equilibrated by 20 ps of constant pressure dynamics at 300K and 1 Atm. Temperature and pressure coupling constants were both 0.2 ps. Production MD simulations for each system were carried out initially for 200 ns following equlibration, at 300K and constant pressure of 1 Atm.

The stability of each trajectory was measured using the root mean squared deviations (RMSD) between the central 5-mers over the whole trajectory against the central 5-mer of the first frame. Half of the structures maintained stable conformations for at least 100 ns at the end of the 200 ns simulations. For structures not reaching a stable conformation in that time frame, the simulations were extended until reaching stability for a continuous 100 ns (Figure S3), which were utilized for energy ranking and further analyses. The MD simulations for the *cis*-B[*a*]P-dG-modified duplexes with partner base at Major-groove, Half-flipped, Flipped and Minor-groove positions achieved stable structural ensembles at 150 – 250 ns, 100 – 200 ns, 225 – 325 ns and 100 – 200 ns respectively for normal partner C; at 150 – 250 ns, 230 – 330 ns, 200 – 300 ns and 100 – 200 ns respectively for mismatched partner T; at 100 – 200 ns for all starting positions of mismatched partner A; and at 260 – 360 ns, 100 – 200 ns, 205 – 305 ns and 275 – 375 ns respectively for mismatched partner G (Figure S3). For a given partner base, in many but not all cases, the stable conformations that evolved from the four starting models converged.

Free energy analyses

The four stable ensembles for each partner were energy-ranked using the molecular mechanics Poisson−Boltzmann surface area (MM-PBSA) method (13) with AMBER9 (6) for the central 5-mers of the 100 ns stable structural ensembles, using 1000 frames at a 100 ps interval of each simulation. The solvation free energy was calculated using the DelPhi program (14), and the solute entropies were estimated with normal mode analysis in AMBER9 (6). The preferred conformation for each partner was selected based on the MM-PBSA energy.

Van der Waals interaction energies

The anal module of AMBER9 (6) was employed to compute van der Waals interaction energies. This energy was computed for two systems. (1) The total interaction energy involving the intercalation pocket: the B[*a*]P aromatic ring system, the adjacent base pairs and the partner base. The identity of the partner base produces differences in these energies as shown in Figure 1 of the main text. Block averages for this case were computed as described below. (2) The van der Waals interaction energy between the partner base and the base pairs adjacent to the B[*a*]P rings was used to determine populations of inserted states for partners A and G as shown in Figure S8.

The raw time series data of van der Waals interaction energies produced by computational MD simulations are series of correlated data. In order to obtain averages and the variances of the averages for these data, we applied the block averaging method (15). In brief, the time series data were divided into “blocks” with a block size that exceeds the longest correlation time, 5 ns in our case. The average for each block was computed and named “block average”. The mean and the standard deviation of the block averages were used to represent the average and the variance of averages.

The block size was determined using the convergence of the standard deviation of the block averages (16). For all raw time series data, we computed the standard deviation of the block averages using a block size from 0.5 ns to 30 ns with an increment of 0.5 ns. The standard deviation values were plotted against the block sizes. The optimal block size was chosen at the point where the standard deviation values converge, reaching a plateau (data not shown). For all our 100 ns time series data, the block size was chosen at 5 ns, resulting in 20 blocks for each time series data.

Hydrogen bond occupancy

The hydrogen bond occupancy (the percent of the time that a given hydrogen bond was present) involving the partner base and nearby DNA residues was calculated using the CARNAL module of AMBER 7 (17). The cut off values were set at 3.2 Å for instantaneous donor (D) – acceptor (A) distance (d_{DA} <= 3.2Å) and 150˚ for instantaneous D–H…A bond angle ($\Theta_{D\text{-}H\ldots A}$ <= 150˚).

Most representative structure

The most representative structure is the frame in an ensemble, which has a conformation closest to all other frames and was obtained using the ptraj module of the AMBER10 suite of programs (18) with the rms distance metric for the central trimers.

PyMOL (Delano Scientific, LLC) was employed to make molecular images and movies.

SUPPORTING RESULTS

Energy ranking of all conformers and characterization of the less probable conformations for the partner nucleotide of each *cis*-B[*a*]P-dG-modified duplex.

The cis-B[a]P-dG:dC duplex. MD simulations starting from three initial positions (major-groove, half-flipped and flipped) converged to similar major groove conformations (Figure S5), while the MD simulation starting from the minor-groove position stabilizes in a minor groove conformation (Figure S4A). However, the MM-PBSA free energy ranking showed that the minor groove conformation is ~ 10 kcal/mol higher in energy than the most favored major groove one (Table S2). In the minor groove conformation, the partner dC, in *anti* glycosidic bond conformation, is displaced into the minor groove, interacting with the backbone of its own strand along the minor groove wall (Figure S4A). The close interactions between the partner C and the minor groove walls stabilize its position in the minor groove, providing some stability to this conformation. However, this conformation of the partner dC exposes the B[*a*]P rings partly to the solvent from the major groove side and leaves the lesion intercalation site somewhat solvent-accessible (Figure S4A).

The cis-B[a]P-dG:dT duplex. MD simulations starting from the half-flipped and flipped positions converged to a major groove conformation (Figure S7); the MD simulation starting from the major-groove position evolved into a ruptured duplex with a free energy of ~ 27 kcal/mol higher than that of the major groove one, and the MD simulation starting from the minor-groove position stabilized in a minor groove conformation (Figure S4B) with a free energy of ~ 2 kcal/mol higher than that of the major groove one. Since the free energy of the minor groove conformation is higher than that of the major groove one, and the latter was reached from two initial structures, the major groove conformation is the preferred one for the *cis*-B[*a*]P-dG:dT duplex (Table S2). In the minor groove conformation, the partner dT, in *syn* glycosidic bond conformation, is displaced into the minor groove: the partner dT forms three hydrogen bonds with nearby residues, while the methyl group of the T that is exposed to the solvent crowds the B[*a*]P benzylic ring (Figure S4B). The crowded T in the minor groove bends the duplex further towards the major groove side. The B[*a*]P rings are slightly exposed to the solvent from the major groove side (Figure S4B).

The cis-B[a]P-dG:dA duplex. MD simulations starting from the major-groove and half-flipped positions converged into a major groove contacting / inserted conformation (Figure S9), while the MD simulations starting from flipped and minor-groove positions converged into a minor groove conformation (Figure S4C) with free energy of ~ 5 kcal/mol higher than that of the major groove one. Hence, the major groove contacting / inserted conformation is the preferred structure. In the minor groove conformation, the partner dA adopts the *anti* glycosidic bond conformation and is displaced into the minor groove: the partner dA forms two hydrogen bonds with nearby residues and provides ring overlaps with the B[*a*]P rings from the minor groove side (Figure S4C). The close interactions with nearby residues stabilize partner dA in the minor groove, which works as a spacer between the backbones of the minor groove walls, bends the duplex further towards the major groove side. The B[*a*]P rings are slightly exposed to the solvent from the major groove side (Figure S4C).

The cis-B[a]P-dG:dG duplex. MD simulations starting from all four positions converged into a major groove contacting / partly inserted conformation (Figure S10).

REFERENCES

1. Chen, Y., Kropachev, K.Y., Liu, Z., Kolbanovsky, M. and Geacintov, N.E. (2010), Human NER recognition mechanisms involving the undamaged strand of the double helix. Presented at the *240th American Chemical Society National Meeting*, Boston, MA. August 24th Poster TOXI 89.
2. Huang, X., Colgate, K.C., Kolbanovskiy, A., Amin, S. and Geacintov, N.E. (2002) Conformational changes of a benzo[*a*]pyrene diol epoxide-*N*(2)-dG adduct induced by a 5'-flanking 5-methyl-substituted cytosine in a (Me)CG double-stranded oligonucleotide sequence context. *Chem. Res. Toxicol.*, **15**, 438-444.
3. Altona, C. and Sundaralingam, M. (1972) Conformational analysis of the sugar ring in nucleosides and nucleotides. A new description using the concept of pseudorotation. *J. Am. Chem. Soc.*, **94**, 8205-8212.
4. MATLAB 7.10.0 (R2010a) ed. The MathWorks, Inc., Natick, MA.
5. Cosman, M., De los Santos, C., Fiala, R., Hingerty, B.E., Ibanez, V., Luna, E., Harvey, R., Geacintov, N.E., Broyde, S. and Patel, D.J. (1993) Solution conformation of the (+)-*cis*-*anti*-[BP]dG adduct in a DNA duplex: intercalation of the covalently attached benzo[*a*]pyrenyl ring into the helix and displacement of the modified deoxyguanosine. *Biochemistry*, **32**, 4145-4155.
6. Case, D.A., Darden, T.A., Cheatham, T.E., III, Simmerling, C.L., Wang, J., Duke, R.E., Luo, R., Merz, K.M., Pearlman, D.A., Crowley, M., Walker, R.C., Zhang, W., Wang, B., Hayik, S., Roitberg, A., Seabra, G., Wong, K.F., Paesani, F., Wu, X., Brozell, S., Tsui, V., Gohlke, H., Yang, L., Tan, C., Mongan, J., Hornak, V., Cui, G., Beroza, P., Mathews, D.H., Schafmeister, C., Ross, W.S. and Kollman, P.A. (2006), AMBER9. University of California San Francisco, San Francisco, CA.
7. Cornell, W.D., Cieplak, P., Bayly, C.I., Gould, I.R., Merz, K.M., Ferguson, D.M., Spellmeyer, D.C., Fox, T., Caldwell, J.W. and Kollman, P.A. (1995) A second Generation Force Field for the Simulation of Proteins, Nucleic Acids, and Organic Molecules. *J. Am. Chem. Soc.*, **117**, 5179-5197.
8. Wang, J.M., Cieplak, P. and Kollman, P.A. (2000) How well does a restrained electrostatic potential (RESP) model perform in calculating conformational energies of organic and biological molecules? *J. Comput. Chem.*, **21**, 1049-1074.
9. Perez, A., Marchan, I., Svozil, D., Sponer, J., Cheatham, T.E., 3rd, Laughton, C.A. and Orozco, M. (2007) Refinement of the AMBER force field for nucleic acids: improving the description of alpha/gamma conformers. *Biophys. J.*, **92**, 3817-3829.
10. Wang, J., Wolf, R.M., Caldwell, J.W., Kollman, P.A. and Case, D.A. (2004) Development and testing of a general amber force field. *J. Comput. Chem.*, **25**, 1157-1174.
11. Mocquet, V., Kropachev, K., Kolbanovskiy, M., Kolbanovskiy, A., Tapias, A., Cai, Y., Broyde, S., Geacintov, N.E. and Egly, J.M. (2007) The human DNA repair factor XPC-HR23B distinguishes stereoisomeric benzo[*a*]pyrenyl-DNA lesions. *The EMBO J.*, **26**, 2923-2932.
12. Berendsen, H.J.C., Postma, J.P.M., Vangunsteren, W.F., Dinola, A. and Haak, J.R. (1984) Molecular Dynamics with Coupling to an External Bath. *J. Chem. Phys.*, **81**, 3684-3690.
13. Kollman, P.A., Massova, I., Reyes, C., Kuhn, B., Huo, S., Chong, L., Lee, M., Lee, T., Duan, Y., Wang, W. *et al.* (2000) Calculating structures and free energies of complex molecules: combining molecular mechanics and continuum models. *Acc. Chem. Res.*, **33**, 889-897.
14. Honig, B. and Nicholls, A. (1995) Classical electrostatics in biology and chemistry. *Science*, **268**, 1144-1149.
15. Flyvbjerg, H. and Petersen, H.G. (1989) Error-Estimates on Averages of Correlated Data. *J. Chem. Phys.*, **91**, 461-466.
16. Yang, W., Bitetti-Putzer, R. and Karplus, M. (2004) Free energy simulations: Use of reverse cumulative averaging to determine the equilibrated region and the time required for convergence. *J. Chem. Phys.*, **120**, 2618-2628.
17. Case, D.A., Pearlman, D.A., Caldwell, J.W., Cheatham, T.E., III, Wang, J., Ross, W.S., Simmerling, C.L., Darden, T.A., Merz, K.M., Stanton, R.V., Cheng, A.L., Vincent, J.J., Crowley, M., Tsui, V., Gohlke, H., Radmer, R.J., Duan, Y., Pitera, J., Massova, I., Seibel, G.L., Singh, U.C., Weiner, P.K., Kollman, P.A. . (2002), AMBER7. University of California San Francisco, San Francisco, CA.
18. Case, D.A., Darden, T.A., Cheatham, T.E., 3rd, Simmerling, C.L., Wang, J., Duke, R.E., Luo, R., Crowley, M., Walker, R.C., Zhang, W., Merz, K. M., Wang, B., Hayik, S., Roitberg, A., Seabra, G., Kolossváry, I., Wong, K. F., Paesani, F., Vanicek, J., Wu, X., Brozell, S. R., Steinbrecher, T., Gohlke, H., Yang, L., Tan, C., Mongan, J., Hornak, V., Cui, G., Mathews, D. H., Seetin, M. G., Sagui, C., Babin, V., and Kollman, P. A. (2008). AMBER10. University of California San Francisco, San Francisco, CA.